Article

NaNO3/NaCl oxidant and Polyethylene glycol (PEG) capped gold nanoparticles (AuNPs) as a novel green route for AuNPs detection in electrochemical biosensors

Adaris M. Lopez-Marzo, Raquel Hoyos-de-la-Torre, and Eva Baldrich

Anal. Chem., **Just Accepted Manuscript** • DOI: 10.1021/acs.analchem.7b05150 • Publication Date (Web): 02 Mar 2018

$NaNO_3$/NaCl oxidant and Polyethylene glycol (PEG) capped gold nanoparticles (AuNPs) as a novel green route for AuNPs detection in electrochemical biosensors

Adaris M. López-Marzo[1], Raquel Hoyos-de-la-Torre[1] and Eva Baldrich[1,2]*

[1] *Diagnostic Nanotools Group, CIBBIM-Nanomedicine. Vall d'Hebron Hospital Research Institute (VHIR). Universitat Autònoma de Barcelona. Passeig Vall d'Hebron 119-129; 08035 Barcelona, Spain.*

[2] *CIBER de Bioingeniería, Biomateriales y Nanomedicina (CIBER-BBN), Spain.*

*Corresponding author: eva.baldrich@vhir.org *Phone: (+34) 934 893 000 (Ext. 3754)*

ABSTRACT: Gold nanoparticles (AuNPs) have been exploited as signal-producing tags in electrochemical biosensors. However, the electrochemical detection of AuNPs is currently performed using corrosive acid solutions, which may raise health and environmental concerns. Here, oxidant salts, and specifically the environmentally friendly and occupational safe $NaNO_3$/NaCl mixture, have been evaluated for the first time as potential alternatives to the acid solutions traditionally used for AuNPs electrooxidation. In addition, a new strategy to improve the sensitivity of the biosensor through PEG-based ligand exchange to produce less compact and easier to oxidize AuNPs immunoconjugates is presented too. As we show, the electrochemical immunosensor using $NaNO_3$/NaCl measurement solution for AuNPs electrooxidation and detection, coupled to the employment of PEG-capped nanoimmunoconjugates, produced results comparable to classical HCl detection. The procedure developed was next tested for human matrix metallopeptidase-9 (hMMP9) analysis, exhibiting a 0,18-23 ng/mL linear range, a detection limit of 0,06 ng/mL, and recoveries between 95 and 105% in spiked human plasma. These results show that the procedure developed is applicable to the analysis of protein biomarkers in blood plasma and could contribute to the development of more environmentally-friendly AuNPs-based electrochemical biosensors.

Nanomaterials (NMs) have provided numerous advantages to electrochemical biosensors for environmental and industrial monitoring, food safety and clinical diagnostic applications, including the achievement of low limits of detection (LoD).[1–3] Thanks to their large surface area and high loading capacity, several signal enhancement strategies have been reported making use of NMs as carriers of multiple signal molecules and biorecognition elements.[1-4] Since many NMs are electrochemically active (e. g. metal nanoparticles), they have also been used as electroactive tracers to produce nanostructured electrochemical transducers of enhanced performance and as catalysts that possess ready availability of active sites on their surfaces.[5–7] Gold nanoparticles (AuNPs) have probably been the NM most extensively used in biosensors because of their rapid and simple chemical synthesis, with control of the shape and narrow size distribution, biocompatibility and easy bioconjugation.[8,9] In the case of electrochemical biosensors, AuNPs present special interest thanks to their unique electrochemical properties that makes possible the development of a large variety of biosensors.[4,9]

The majority of the AuNP-based electrochemical biosensors published to date reports the use of AuNPs either as carriers of electrochemical tags and/or analyte bioreceptors, or as modifiers of the electrode surface, often associated with polymers, graphene or combined with other NMs.[3-8] However, there are less works focused on the use of AuNPs as electroactive label in comparison with other metal NPs largely exploited as signal tags (AgNPs, CdS and CdSe quantum dots, etc).[5,10] Nevertheless, efficient AuNPs based detection strategies using differential pulse voltammetry (DPV),[11–15] square wave voltammetry (SWV), anodic stripping voltammetry,[16–22] chronoamperometric monitoring of the hydrogen evolution reaction,[23–25] and electrochemical impedance spectroscopy (EIS)[26] have been described on carbon paste,[14,17,27] graphite–epoxy electrodes,[11] pencil graphite electrodes (PGE)[20] and screen printed carbon electrodes (SPCE).[13, 15,21–26,] Biosensors using AuNPs as signal generators have been developed to detect *E. coli* bacteria cells,[16,25] α-elonase (ENO1),[21] specific DNA amplified sequence,[18,20] human IgG (HIgG)[12,15] and human serum albumin (HSA)[13] in serum samples. Magnetic beads have also been used as biosensor platforms coupled to the use of AuNPs,[23,26,28] while the effect of the AuNPs size on the electrochemical signal has been studied too.[28] In all these biosensors, the authors use corrosive acid solutions (HBr/Br_2[18] mixture or HCl[11-28]) for the electrooxidation of the $AuNPs^0$ tags to Au^{3+}. This is then followed by the electrochemical reduction of Au^{3+} to Au^0 at the electrode surface, which is either directly determined by DPV or SWV as a well-defined peak, or indirectly monitored by chronoamperometric or impedimetric detection of hydrogen evolution catalyzed by the AuNPs. Nonetheless, the employment of an acidic reagent raises environmental and safety concerns, and may discourage the implementation of this type of detection strategy at point-of-care settings.[29]

Here, for the first time, non-acid oxidants have been evaluated for the electrochemical oxidation of AuNPs in substitution of the acid solution. Among the products tested, the environmentally friendly $NaNO_3$/NaCl mixture has been selected for developing a new AuNPs detection method. The concept of AuNPs ligand exchange to produce a conjugate easier to oxidize, as an effective route to increase immunosensor sensitivity, has been introduced here for the first time too. As it is shown, the use of $NaNO_3$/NaCl as the oxidant coupled to PEG-capped AuNPs offered a novel synergic strategy that provided a biosensor response similar to that obtained using citrate-stabilized AuNPs and HCl as the oxidant. The performance of the new immunosensing strategy has been finally

demonstrated by detecting human matrix metallopeptidase-9 (hMMP9) in spiked samples of human pooled plasma. MMP9 is a protease involved in the breakdown of extracellular matrix in numerous physiological processes that is over expressed in pathologies such as arthritis, cardiovascular, neurological and some cancers.[30] The developed immunosensor presented a lineal range from 0,18 to 23 ng/mL of hMMP9, with a LoD of 0,06 ng/mL. The recoveries found during the accuracy assay in plasma were of 95-105% in the 1,25-15 ng/mL analytical range. The results suggest that the electrochemical immunosensor produced here fits the requirements for the analysis of protein biomarkers in blood plasma. Furthermore, both the use of $NaNO_3$ oxidant as a more environmental friendly and occupational safer alternative than acid and the ligand exchange on the gold surface to increase the sensitivity of the immunosensor could contribute to the development of a renewed type of signal gold-based electrochemical biosensors and offer new paths for these assays.

EXPERIMENTAL SECTION

Chemicals and Biocomponents

Citrate-stabilized AuNPs (AuNPs/citrate, 20 nm diameter), rabbit IgG (RIgG), goat anti-rabbit IgG (Goat@RIgG, whole molecule), bovine serum albumin (BSA), HCl 37% (v/v, trace metal grade), polyethylene glycol (PEG; 400 g/mol average molecular weight), potassium ferrocyanide ($K_4[Fe(CN)_6]\cdot 3H_2O$), lithium perchlorate ($LiClO_4$), sodium nitrate ($NaNO_3$) and sodium chloride (NaCl) were purchased from Sigma-Aldrich. The hMMP9, anti-hMMP9 goat polyclonal antibody (Goat@hMMP9; antigen affinity-purified), and anti-hMMP9 mouse monoclonal Ab (Mouse@hMMP9) were acquired from R&D Systems. Human pooled plasma was supplied by H2B. Phosphate buffered saline (PBS) tablets, Tween 20, and potassium ferricyanide ($K_3[Fe(CN)_6]$) were purchased from Gibco, Fischer Scientific and Acros Organics, respectively.

Electrochemical measurements

Cyclic voltammetry (CV) and DPV were performed using a CH Instruments 1030C multipotenciostat. SPCE (ref. 110; DropSens, Llanera, Spain) comprised carbon counter and working electrodes (WE, d = 4 mm), and silver pseudoreference electrode. Before their utilization, SPCE were characterized by CV (from -0,2 to 0,45 V at 0,1 V/s) using 0,1 mM $K_4Fe(CN)_6$ in 0,1 M KCl.

For the optimization of AuNPs electrochemical detection, 10 µL (0,05 or 0,1 nM) of AuNPs or AuNPs-Ab-BSA conjugate were deposited on the WE and DPV measurements were registered in 60 µL of 0,1 M HCl (E_i=1,0 - 1,3 V; 3-180 s of electrooxidation). In the assays carried out on the immunosensor platform, a typical electrochemical measurement included previous AuNPs electrooxidation at 1,1 V during 60 s in 0,5 M HCl (40 µL). The $[AuCl_4]^-$ oxidized specie produced in this way was next detected by DPV scanning from 1,1 to -0,1 V (0,02 s pulse width and 0,1 V pulse amplitude).

Ligand exchange of AuNPs/citrate to produce AuNPs/PEG

Briefly, 500 µL of AuNPs/citrate were mixed with 1 mL of 0,25% PEG (v/v) aqueous solution under agitation for 18 h. The PEG excess and the replaced citrate were removed by centrifugation (15 min, 11ºC and 16 rcf) and AuNPs/PEG were washed with H_2O-0,05% Tween 20 (850 µL) and resuspended in Milli-Q H_2O (500 µL).

Production of the nanoimmunoconjugates

Gold nanoimmunoconjugates were produced by incubating 500 µL of AuNPs/citrate or AuNPs/PEG (1,2 nM) with 113 µL of detection Ab (40 µg/mL of either RIgG or Goat@hMMP9) with gentle agitation for 30 min, followed by blocking with PBS-0,1% BSA (500 µL) for 30 min. The conjugate (either AuNPs-RIgG-BSA or AuNPS-Goat@hMMP9-BSA) was washed with PBS-Tween 20 0,05% by centrifugation for 15 min at 11 °C and 16 rcf, and was resuspended in PBS-0,2% BSA for storage at 4ºC.

Characterization of AuNPs and their nanoimmunoconjugates

The dynamic light scattering (DLS) and zeta potential measurements of an aqueous solution of AuNPs or gold nanoimmunoconjugate were carried out using a Malvern Zetasizer NanoSeries at room temperature. Transmission electron microscopy (TEM) images were recorded after just drying 5 µL of the conjugates aqueous solution on holey *carbon* coated grids using a Tecnai F20 HRTEM/STEM. UV-Vis spectra were recorded on a Cary 60 UV-Vis spectrophotometer (Agilent Technologies). RMN spectra were recorded on a 400 MHz Bruker AV3-400SB spectrometer. For these studies, 16 mL of AuNPs/ligand were washed four-times with Milli-Q H_2O, dried and dissolved in 500 µl of D_2O (38 nM AuNPs).

Preparation of the immunosensors

Two immunosensor formats were used. The first one, SPCE/Goat@RIgG-BSA/AuNPs-RIgG-BSA, was used as a model system to carry out the optimization of the different biosensor components (Figure 1A). The second one, SPCE/Mouse@hMMP9-BSA/hMMP9/AuNPs-Goat@hMMP9-BSA, was next employed to demonstrate the applicability of the system to detection of hMMP9 as an analyte of clinical interest (Figure 1B).

All incubations were carried out inside a humid chamber to prevent evaporation and were followed by two washes with PBS-Tween 20 (0.05%) and one wash with PBS.

In the SPCE/Goat@RIgG-BSA/AuNPs-RIgG-BSA format, the WE was modified overnight with 10 µL (6,25; 12,5; 25 or 40 µg/mL) of capture Ab (Goat@RIgG), was next blocked with PBS-BSA (0,1 or 0,2%) during 30 min and was finally incubated with 35 µL (0; 0,3; 0,6; 1,2 and 2,4 nM) of the AuNPs-RIgG-BSA conjugate for 30 min under shaking (25 or 50 rpm).

For hMMP9 determination, based on the SPCE/Mouse@hMMP9-BSA/hMMP9/AuNPs-Goat@hMMP9-BSA sandwich, 10 µL (40 µg/mL) of capture Ab (Mouse@hMMP9) were used to functionalized the WE, followed by blocking with 0.2% BSA. After that, 140 µL of the AuNPs-Goat@hMMP9-BSA conjugate were incubated with 3,5 µL of hMMP9 (0,18 to 30 ng/mL) for 30 min. Then, 35 µL of this mixture were incubated for other 30 min with the SPCE/Mouse@hMMP9-BSA for the second immunorecognition. In both formats, 40 µL of 0,5 M HCl or $NaNO_3$/NaCl were alternatively used as the electrochemical measurement solution.

Data Analysis

The limits of detection and quantification (LoD and LoQ) were calculated by dividing the standard deviation of the regression line intercept (S_a) by the slope of the calibration curve (b) as determined by the equations 1 and 2, respectively.[31]

$$X_{LoD} = \frac{3S_a}{b} \qquad (1)$$

$$X_{LoQ} = \frac{10S_a}{b} \qquad (2)$$

The sensitivity corresponded to the slope of the calibration curve in the lineal range.

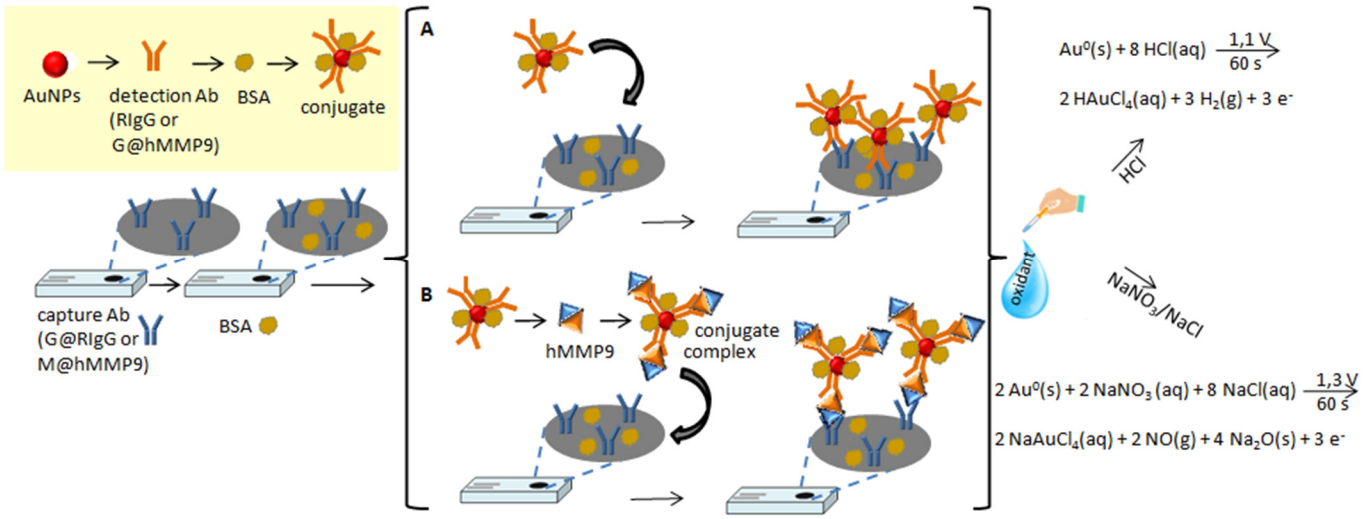

Figure 1. Scheme of preparation of the two immunosensors used and their analytical working principle. A) SPCE/Goat@RIgG/BSA/AuNPs-RIgG-BSA model system and B) SPCE/Mouse@hMMP9-BSA/hMMP9/AuNPs-Goat@hMMP9-BSA for hMMP9 detection.

RESULTS AND DISCUSSION

Optimization of the AuNPs electrochemical detection conditions on bare SPCE by classical acidic electrooxidation

As is known, gold presents one of the highest oxidation potentials (E^o = +1,35 V) displayed by chemical species. It is thus necessary to perform the electrooxidation of Au^0 into Au^{3+} (usually at E_i=1,2 - 1,4 V in 1 - 2 M HCl) previous to the subsequent measurement of the gold reduction.[11-28] Here, we studied the reduction peak heights generated by both bare AuNPs and a AuNPs-RIgG-BSA nanoimmunoconjugate at unmodified SPCE, after HCl electrooxidation for increasing times and potentials.

The electrochemical response produced by AuNPs was twice higher than that registered for the AuNPs-RIgG-BSA conjugate (Figures 2A and S2). This could be explained because in the conjugate the gold surface has lower exposure to the acid action for the oxidation process, as well as poorer diffusion of the oxidized specie formed, $[AuCl_4]^-$, towards the electrode surface.

As summarized in Figure 2A, for electrooxidation potentials between 1 and 1,1 V, both AuNPs and AuNPs-RIgG-BSA produced reduction peaks of similar height independently of the electrooxidation time. When increasing the potential to 1,2 and 1,3 V, the signal current registered increased with the electrooxidation time. However, this increment in oxidation potential and time also produced the arising of a second broad peak between 0,6 and 0,8 V that interfered in the quantification of the AuNPs analytical peak (Figure S1 A). Since this interfering peak, which was SPCE batch-dependent, appeared also when using metal traces grade HCl, it was concluded that it originated from the SPCE itself after exposure to HCl at potentials ≥ 1,2 V for times ≥ 10 s (Figure S1 B). Previous works also made reference to damage caused on the SPCE surface and its further effect in the DPV signal when high voltages and long times of oxidation were applied in acid solutions.[12,15] Accordingly, we carried out AuNPs DPV electroxidation at 1,1 V for 60 s, in order to guarantee the best ratio between high current peak and good repeatability. In consequence, we tried to improve detection sensitivity by optimizing other parameters in the immunosensor format.

Optimization of the model immunosensor

The optimization of the immunosensor platform was first carried out with the SPCE/G@RIgG-BSA/RIgG-AuNPs-BSA format as a model system (Figure 1A). In this model system, increasing concentrations of the AuNPs-RIgG-BSA conjugate were incubated on the SPCE/Goat@RIgG-BSA for immunocapture. As the AuNPs have the double function of carrier of multiple detection Abs and electroactive label, the peak current measured was proportional to the concentration of electrode surface-confined conjugate. In these experiments, the conjugate was diluted in PBS-0,1/0,2% BSA in order to approximate the characteristics of human plasma. Since the total protein content in human plasma is of 5-8%, plasma diluted 1/40 plasma would display 0,1-0,2% of protein.

Concerning the effect of the HCl concentration, Figure S3 shows that when 0,1 and 0,5 M of HCl were used alternatively to detect increasing concentrations of the RIgG-AuNPs-BSA conjugate, the immunosensor displayed wider linear range, extending to higher conjugate concentrations, for 0,5 M HCl. This suggested that 0,1 M HCl was insufficient to oxidize the highest conjugate concentrations tested here. On the other hand, the stability studies demonstrated that the nanoimmunoconjugate was stable for up to 8 days of storage at 4°C, which allowed preparing relatively large quantities of this reagent, facilitating the experimental work (Figure S4).

As expected, an increase of the concentration of capture Ab used to modify the WE surface from 6,25 to 40 µg/mL produced an improvement in the currents measured and the immunosensor sensitivity, as indicated by the slopes of the calibration curves, because of the binding of a higher amount of conjugate (Figure 2B). Figure S5 shows that, for the concentrations of capture Ab tested, there was not notable difference in sensor response between the use of 0,2 and 0,1% of BSA as the blocking solution. Therefore, we decided to use 0,2% BSA to provide better electrode blocking without compromising sensor sensitivity.

The effect of the agitation rate during the immunocapture reaction was finally studied. We found that raising the agitation speed from 25 to 50 rpm produced a 2-fold increase in the electrochemical response, as well as sensitivity improvement from 25 to 50 µA/nM (Figure 2C). It is known that the increase of the agitation rate contributes to accelerate convective diffusion during the incubation and facilitates the mass transfer from the bulk solution to the sensor surface. Consequently, more collisions occur between the capture and detection Abs, which increases the probability to generate effective collisions that will lead to immunobinding.

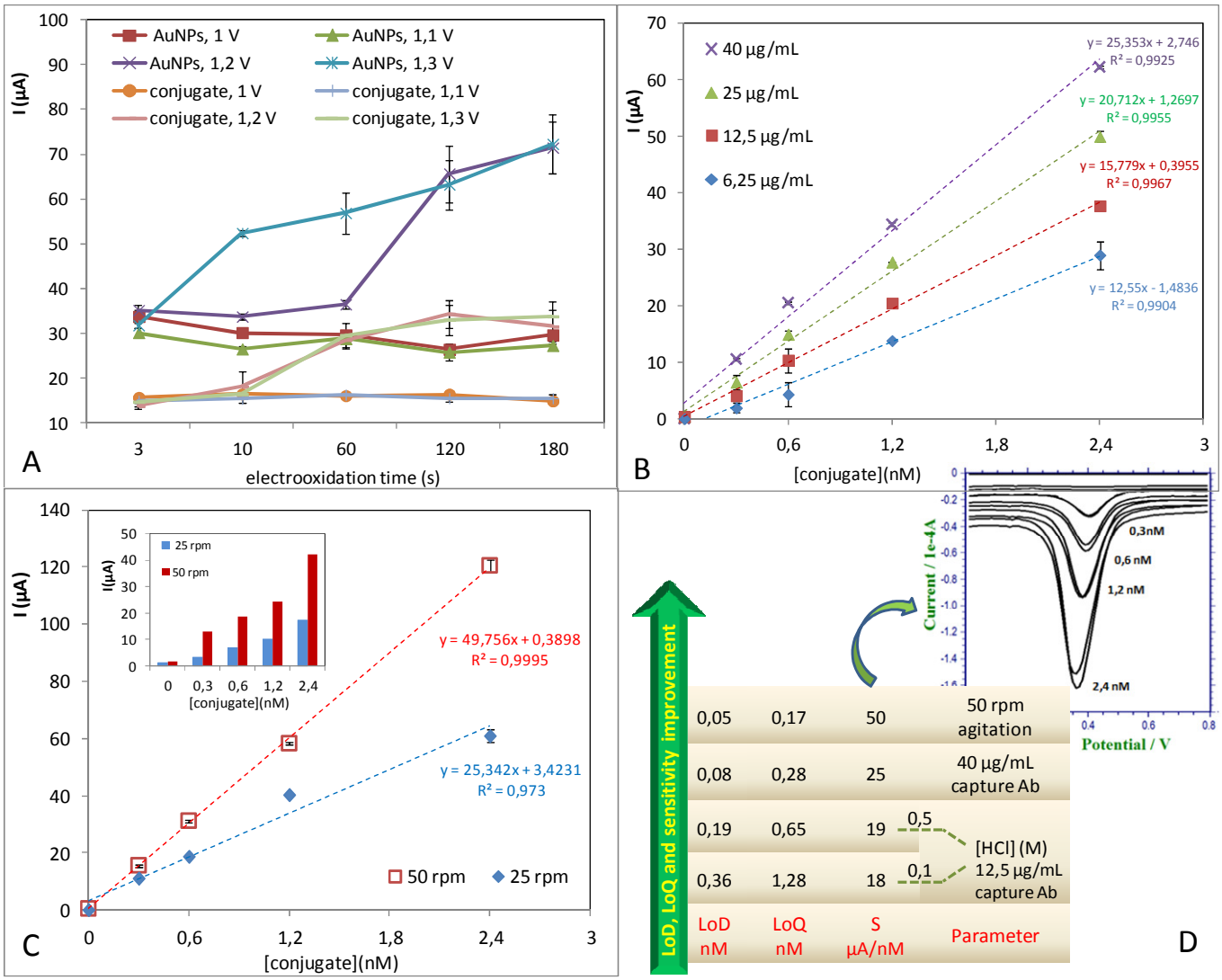

Figure 2. Study of AuNPs electrochemical detection conditions on bare SPCE. A) Effect of different AuNPs electrooxidation potentials and times on the DPV peaks currents registered for 0,1 nM of AuNPs and AuNPs-RIgG-BSA conjugate. Optimization of the model immunosensor [WE/Goat@RIgG-BSA/AuNPs-RIgG-BSA/0,5 M HCl]. Effect on immunosensor response of, (B) the concentration of Goat@RIgG capture Ab used to modify the WE (0,1% BSA in the blocking solution) and, C) the agitation rate during the immunocapture process (40 µg/mL of capture Ab, 0,2% BSA). D) Summary of the results obtained during these optimizations in terms of improvement of the LoD, LoQ and sensitivity. Insert) DPVs registered for increasing conjugate concentrations under optimized immunosensor conditions (2 independent replicates are shown per concentration).

The scheme in Figure 2D summarizes the improvement registered for some of the optimizations discussed before. These results illustrate clearly how the electrochemical signal can be ameliorated, achieving a 10-fold improvement in the LoD (from 0,4 to 0,05 µA/nM) and LoQ (from 1,28 to 0,17 µA/nM), by just optimizing some simple variables in the system. Upon optimization, the procedure included modification of the SPCE with 40 µg/mL of Goat@RIgG capture Ab, blocking with 0.2% BSA, AuNPs-RIgG-BSA conjugate incubation at 50 rpm, and electrochemical detection by DPV in HCl 0,5 M. Under these experimental conditions, a 1,2 nM conjugate concentration provided a reduction peak of about 60 µA by DPV (see the insert in Figure 2D).

$NaNO_3$ as an environmentally friendly alternative for the electrochemical oxidation of AuNPs

As mentioned before, HBr/Br_2[18] mixture and HCl[11-28] have been used for dissolving and oxidizing gold in all the electrochemical biosensors with AuNPs detection. The concentrations of HCl used in these assays (often 1-2 M, equivalent to 36500-73000 ppm and pH <0.3) are high if we consider the concentration limits set by the Environmental Protection Agency (EPA) for the occupational safety (5 ppm in air for 8 h of work) and the acceptable pH range for environmental wastewater disposal (6-8,5).[29] To our knowledge, an electrochemical biosensor using a non-acidic oxidant, such as $NaNO_3$, $K_3(FeCN)_6$ or $LiClO_4$, has not been reported yet. However it is known that $NaNO_3$/NaCl, $FeCl_3$, and HCl can oxidize gold, since they are reagents used in the auriferous mines ($NaNO_3$, $Fe^{3+}$and H^+ as oxidant agents and chlorine as a gold chelating ligand).[32–34] In addition, by substituting HCl by a non-toxic (or less toxic) oxidant we move towards greener biosensor chemistry, which would be especially relevant for point-of-care handling.

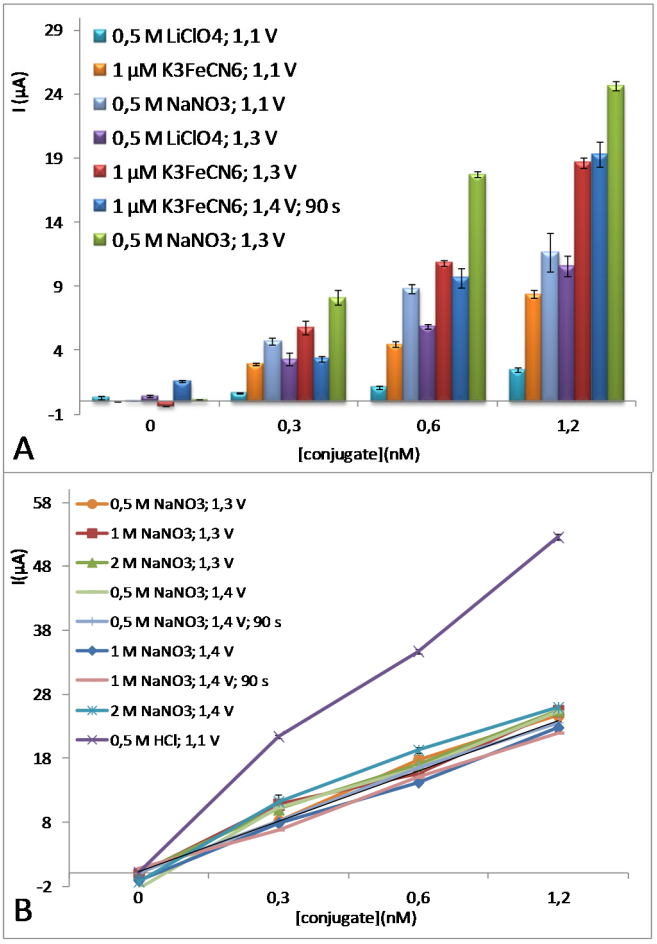

Figure 3. Evaluation of K_3FeCN_6, $LiClO_4$ and $NaNO_3$ non-acid oxidants (in 0,5 M NaCl for all cases) as alternatives to HCl for AuNPs electrooxidation under different electrochemical measurement conditions. A) Electrochemical response obtained using alternatively K_3FeCN_6, $LiClO_4$ and $NaNO_3$ oxidants. B) Reduction currents obtained using as the oxidant either HCl or $NaNO_3$/NaCl. The [WE/40µg/mL G@RIgG-(0,2% BSA)/AuNPs-RIgG-BSA/*x* M] immunosensor format was used in all these assays.

Figure 3A presents the currents obtained in the immunosensor using alternatively $NaNO_3$, K_3FeCN and $LiClO_4$ as oxidants. In all cases, 1,3 V supplied higher currents than 1,1 V, with $NaNO_3$ providing the best results, followed by K_3FeCN_6 and $LiClO_4$. It is important to highlight that the K_3FeCN_6 oxidant was used at very low concentration because above 1 µM, Fe^{3+} produced a reduction peak that overlapped with the Au^{3+} one (Figure S6 A). Attempts to ameliorate the Fe^{3+} detection by increasing the potential and oxidation times (to 1,4 V and 90 s), produced a decrease in the currents measured.

Figure 3B displays the electrochemical responses registered when using increasing concentrations of $NaNO_3$/NaCl (0,5; 1 and 2 M) under different electrooxidation conditions (1,3 and 1,4 V for 60 and 90 s). It was observed that raising the salt concentration and oxidation potential above 0,5 M and 1,3 V, respectively, did not improve the biosensor response. Under these conditions, and in spite of the high working potential and salt concentration, $NaNO_3$ did not generate the interference peak observed when using 0,5 M HCl at similar conditions (Figure S6B). Nonetheless, the use of stronger electrooxidation conditions (90 s at 1,4 V) affected slightly Au quantification by arising the peak evolved from the SPCE surface, even if it was much lower than when working with HCl under similar electrochemical conditions (Figure S6C).

The use of 0,5 M HCl (1,1 V for 60 s) was more effective than 0,5 M $NaNO_3$/NaCl (1,3 V for 60 s) for AuNPs/citrate-based immunoconjugate electrooxidation, and generated reduction peaks nearly two times higher. Nevertheless, $NaNO_3$/NaCl provided nanoimmunoconjugate quantization in all the concentration range tested. Therefore, these results demonstrate that $NaNO_3$/NaCl can be used to substitute HCl, providing a more environmentally-friendly reagent for AuNP electrochemical measurement. Moreover, the decrease in sensitivity observed when using $NaNO_3$/NaCl could be compensated by analyzing samples 2-times more concentrated.

Production and characterization of PEG-capped AuNPs and their nanoimmunoconjugates.

PEG is a non-toxic and low cost polymeric material that is easily assembled with AuNPs, allowing their subsequent functionalization with proteins. Here, PEG was incorporated by performing a ligand exchange on AuNPs/citrate, in an attempt to generate bigger conjugates with a less compacted protein cover that could render the gold surface more accessible to the oxidant solution. For the production of AuNPs/PEG, 1 mL of 0,1; 0,25 and 0,5% PEG aqueous solutions were mixed with 500 µL of AuNPs/citrate under shaking during 3, 6 and 18 h. Figure 4A shows that the extension of the reaction time from 3 to 18 h produced an increase in the z-potential of the AuNPs/PEG for all PEG concentrations tested. It is worth noting that more negative surface charges correlate with improved AuNPs stability in solution caused by electrostatic repulsion. A reaction time of 18 h provided z-potential values above 30 mV (absolute value) as is recommended for good stability of the colloidal liquids.[35]

These values were higher than those determined for the AuNPs/citrate used here, 24,4 ± 5,1 mV, which is in agreement with previous reports.[35] In consequence, the ligand exchange on the AuNPs surface was accomplished after 18 h of reaction time with 0,25% PEG. On the other hand, the DLS measurements carried out on AuNPs/citrate, AuNPs/PEG and their respective nanoimmunoconjugates revealed an increase in the hydrodynamic diameter when citrate was exchanged by PEG on the AuNPs surface (Figure 4B). This could be related to the larger size of the PEG molecule capping the AuNPs compared to citrate. It was also noted that the size distribution of the nanoimmunoconjugates was wider than the corresponding AuNPs cores. Additionally, the DLS measurements showed that aggregate formation was negligible for both bare and immunomodified AuNPs/PEG. A closer inspection of the TEM images revealed a shadow bordering around the gold surface of the AuNPs/PEG immunoconjugate, which was absent in bare AuNPs/PEG and was attributed to the organic coating (Figure 4C-D).[36]

Also, the TEM image in Figure 4E illustrates the absence of aggregates in the solution of AuNPs/PEG-based conjugate. Additional indirect confirmation of the formation of the nanoimmunoconjugates was obtained from the UV-Vis spectra. It is known that the position of the surface plasmon band (SPB) maximum is deeply influenced by AuNPs size and geometry, and by the dielectric constant of the surrounding environment. Here, the presence of proteins anchored onto the surface was indirectly probed by a red-shift of 3 nm in the SPB maximum detected by UV−Vis spectroscopy (Figure S7).[35-37] The NMR analysis performed to AuNPs/citrate and AuNPs/PEG confirmed the citrate-PEG ligand exchange. The AuNPs/PEG ^{1}H-NMR spectra

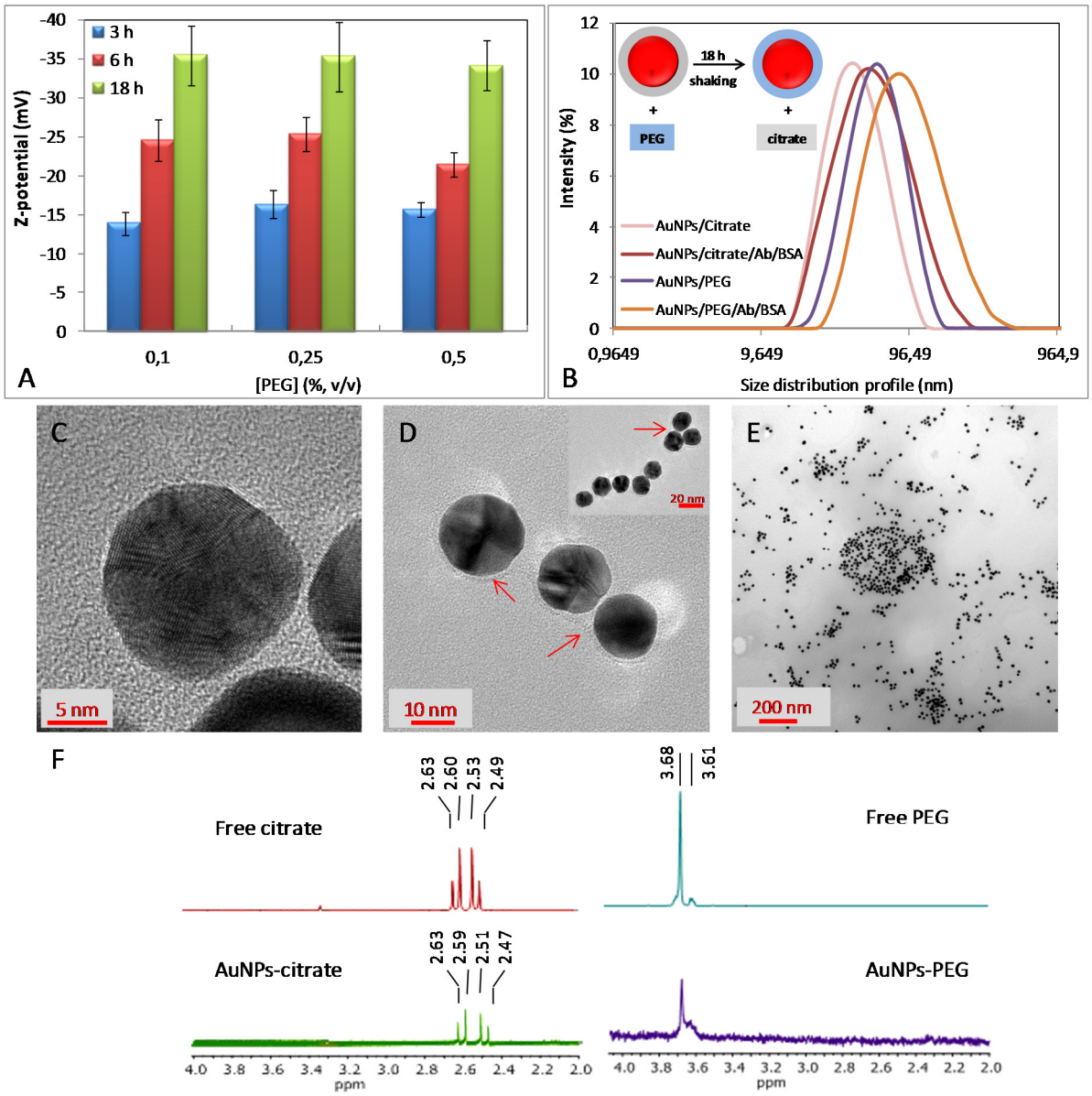

Figure 4. Characterization of the AuNPs/PEG and the corresponding nanoimmunoconjugate. A) z-potentials of AuNPs/PEG obtained after ligand exchange for 3-18 h. B) DLS measurements carried out on AuNPs/citrate, AuNPs/PEG and their corresponding nanoimmunoconjugates. C-E) TEM images of AuNPs/PEG, either bare (C) or immunoconjugated (D-E); the red arrow in D highlights the surrounding shadow attributed to the protein coating. F) ^{1}H-RMN spectra recorded for citrate, AuNPs/citrate, PEG and AuNPs/PEG in D_2O.

displayed the singlet at 3,68 rpm corresponding to the CH_2 groups in PEG ligand, which was absent from the AuNPs/citrate spectra. In addition, the group of peaks associated to the citrate protons do not appear in the corresponding spectral zone of AuNPs/PEG, confirming the successful ligand exchange The peaks' distortion observed in AuNPs-PEG peaks compared with the free PEG ligand can be attributed to some deformation in the structure caused by the interaction with the gold surface, which conducts to structural rigidity and consequently low relaxing times (Figure 4F).[38]

Application of the immunosensing strategy developed to the detection of hMMP9

The detection procedure developed was finally tested for detection of a protein biomarker of clinical interest, hMMP9. In the immunosensor for hMMP9 detection (Figure 1B), a AuNPs-Goat@hMMP9-BSA nanoimmunoconjugate was first incubated with the hMMP9-containg samples, generating a hMMP9/AuNPs-Goat@hMMP9-BSA immunocomplex. This conjugate complex was next captured in a second immunoreaction by the Mouse@hMMP9 mAb immobilized previously onto the WE surface, forming the Mouse@hMMP9/hMMP9/AuNPs-Goat@hMMP9-BSA sandwich. The height of the reduction peak obtained though AuNP electrochemical detection was then correlated to the concentration of hMMP9 in the sample.

Figure 5A shows the calibration curves obtained for detection of hMMP9 in PBS-0,1% BSA, using different combinations of conjugates and electrochemical measurement solutions. As expected, when an AuNPs/citrate-based immunoconjugate and $NaNO_3$ measurement solution were used, the immunosensor sensitivity decreased compared to that using an AuNPs/citrate-based immunoconjugate and HCl.

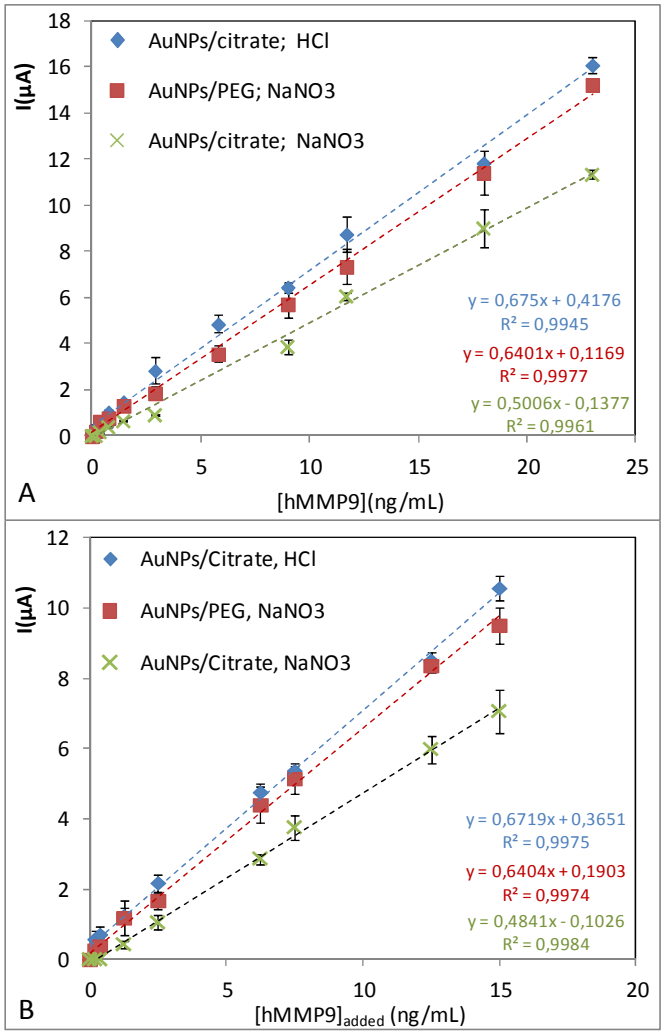

Figure 5. Detection of hMMP9 using different combinations of nano-immunoconjugates (either AuNPs/citrate or AuNPs/PEG based) and oxidant agents (0,5 M of either HCl or $NaNO_3$). The calibration curves were obtained for hMMP9 standard solutions in PBS-0,1%BSA (A) or in spiked human plasma diluted 1:80 and 1:40 (B).

However, when the AuNPs/PEG-based immunoconjugate and $NaNO_3$ were used, the immunosensor displayed similar peak currents, sensitivity and signal-to-noise ratios than those obtained with the AuNPs/citrate-based immunoconjugate in HCl (Figure S8). This behavior could be associated to the bigger size and less compact coating of the conjugate produced via PEG-capped AuNPs, which makes the gold core of the conjugate easier to oxidize, generating higher currents and sensitivity in the immunosensor. PEG has a 2-fold larger molecular weight compared to citrate and a lineal molecular arrangement that might provide surface-protruding spacer arms and a less packed AuNPs cover, which might facilitate the mobility of $[NO_3]^-$ oxidizing and $[AuCl_4]^-$ oxidized molecules towards and from the AuNPs surface.

The immunosensor developed displayed LoD and LoQ around 0,06 and 0,2 ng/mL, respectively (equivalent to $6{,}7x10^{-13}$ and $2{,}0x10^{-12}$ M), lower than other values reported before for electrochemical biosensors using AuNPs as signal tag (Table SI-9).[12,13,22,26,27] The linear range spanned from 0,18 to 23 ng/mL of hMMP9 ($R^2 > 0{,}99$). The variance analysis of the lineal regression revealed that the values calculated for F were higher than the corresponding tabulated value (for α=0,05, n_1=1, n_2=n-2=8 being n the total number of points and n_1 and n_2 the degrees of freedom), which confirms the linearity in the mentioned concentration range (Figure S10).[31]

The immunosensor was finally tested in plasma spiked with hMMP9 concentrations matching those expected in plasma samples from both healthy individuals and patients (20-600 ng/mL).[30,39] For this accuracy study, 3,5 µL of human pooled plasma, spiked with increasing hMMP9 concentrations (0, 15, 100, 500 and 600 ng/mL), were mixed with either 140 µL of the conjugate plus 137 µL of PBS to produce 1:80 plasma dilutions (post-dilution hMMP9 concentrations of 0; 0,188; 1,25; 6,25 and 7,5 ng/mL), or with only 140 µL of the conjugate to produce 1:40 plasma dilutions (post-dilution hMMP9 concentrations of 0; 0,375; 2,5; 12,5 and 15 ng/mL; see experimental scheme in Figure S11 and the currents obtained without correction of the endogenous hMMP9 with 1:80 and 1:40 dilutions plasma in Figure S12). In this way, post-dilution hMMP9 concentrations (0,18-15 ng/mL) fit the lineal range of our immunosensor (0,18-23 ng/mL). The plot of the currents obtained during the accuracy assays versus the concentrations of hMMP9 spiked in both 1:80 and 1:40 plasma dilutions was linear between 1,25 and 15 ng/mL of hMMP9 (equivalent to pre-dilution concentrations ranging 15-600 ng/mL), with sensitivity similar to that observed in the calibration experiments carried out in PBS-0,1% BSA (Figure 5B). This indicated that the immunosensor displayed irrelevant analytical bias when operated in diluted plasma compared to PBS-BSA. Consistently, MMP-9 recovery was around 95-105% for spiked post-dilution concentrations between 1,25 and 15 ng/mL, and of 110-125% for the lowest concentrations tested (Table 1), and spiked and detected MMP-9 concentrations correlated linearly (y=x) with R^2>0,99 (Figure S13). Finally, the concentration of endogenous hMMP9 detected by the immunosensor in pooled plasma was of about 42 ng/mL, which is in agreement with previously reported hMMP9 concentration in healthy individuals.[40]

Table 1. Recoveries obtained for the hMMP9 determination in spiked human pooled plasma (CV between 2 and 10%).

recoveries (%)	hMMP9 spiked concentration (ng/mL), pre-diluted				
	0	15	100	500	600
	hMMP9 spiked concentration (ng/mL), 1/40 dilution				
	$[hMMP9]_{endogenous}$	0,375	2,5	12,5	15
AuNPs/Citrate, HCl	46,7	113,5	104,1	95,9	100,2
AuNPs/PEG, $NaNO_3$	41,4	111,7	97,1	103,1	97,8
AuNPs/Citrate, $NaNO_3$	36,9	-	94,3	97,8	95,2
recoveries (%)	hMMP9 spiked concentration (ng/mL), 1/80 dilution				
	$[hMMP9]_{endogenous}$	0,188	1,25	6,25	7,5
AuNPs/Citrate, HCl	44,7	124,1	98,1	102,8	97,8
AuNPs/PEG, $NaNO_3$	43,5	118,9	98,5	104,2	104,6
AuNPs/Citrate, $NaNO_3$	38,1	-	89,3	95,9	103,7
mean total recoveries	(98,91 ±4,23)% for the analytical range (1,25-15 ng/mL)				

CONCLUSIONS

In this work, oxidizing salts, and specifically $NaNO_3$, have been used for the first time instead of classical acidic dissolution for the electrochemical detection of AuNPs-based nanoimmunoconjugate labels with immunosensing purposes. Additionally, a new strategy to increase the immunosensor sensitivity by producing nanoimmunoconjugates easier to oxidize has been introduced by a PEG ligand exchange on the gold surface. In order to evaluate the real applicability of the new protocol, an immunosensor for hMMP9 detection in human plasma has been developed using AuNPs-based immunoconjuges as the analyte recognition and tag tool. The immunosensor exhibited a linear range from 0,18 to 23

ng/mL, and LoD and LoQ around 0,06 and 0,2 ng/mL, respectively. The recoveries obtained in the accuracy assays in diluted human pooled plasma were between 95-105% over the 1,25-15 ng/mL working range, equivalent to 15-600 ng/mL in pre-diluted plasma, a range that includes the physiological and pathological concentrations of hMMP9 expected in clinical samples (20-600 ng/mL). These results have been achieved taking advantage of the following issues:

- the successful optimization of the components of the immunosensor on a model assay format, achieving a 10-fold improvement in the LoD;
- the assessment of several oxidant salts for the non-acidic electrooxidation of AuNP;
- the use of $NaNO_3$ for the electrochemical detection of AuNPs, which has been demonstrated here for the first time as an environmentally friendly alternative compared to the corrosive acid solutions employed in previous reports;
- and the introduction of the AuNPs citrate-PEG ligand exchange to produce a AuNPs/PEG-based immunonanoconjugate less compact and with gold surface easier to oxidize, which coupled to the use of $NaNO_3$/NaCl as the electrochemical measurement improved the electrochemical immunosensor response, providing current values similar to those obtained when using AuNPs/citrate-based nanoimmunoconjugate and HCl.

The two last aspects could be relevant also for the development of novel biosensors based on the detection of AuNPs employing other electrochemical methods and electrode types. Moreover, moving towards the production of green and successful biosensor platforms fits the social demand for safe, efficient and sustainable diagnostic tools.

ASSOCIATED CONTENT

Supporting Information

A Supporting Information file is available free of charge on the ACS Publications website and includes DPV profiles of the peaks registered under different electrochemical conditions, results of the immunosensor optimizations, stability of the conjugate, UV-Vis spectra of the AuNPs-based conjugates, scheme and results of the accuracy assay, and other additional information.

AUTHOR INFORMATION

Corresponding Author

* E-mail: eva.baldrich@vhir.org, phone: +34934893000 (ext. 3754)

ORCID

E. Baldrich: 0000-0003-1393-215X
A. López_Marzo: 0000-0001-8552-8637

Notes: The authors declare no competing financial interest.

ACKNOWLEDGMENTS

Work was funded by project grant PMP15-00022; EB and ALM are supported by the Miguel Servet and the Sara Borrell programs, respectively (grants CP13-00052 and CD16/00244). The three grants were funded by the *Instituto de Salud Carlos III*, co-financed by the European Regional Development Fund (ERDF).

REFERENCES

(1) Lan, L.; Yao, Y.; Ping, J.; Ying, Y. *Biosens. Bioelectron.* **2017**, *91*, 504–514.
(2) Farka, Z.; Juřík, T.; Kovář, D.; Trnková, L.; Skládal, P. *Chem. Rev.* **2017**, *117*, 9973–10042.
(3) Zhu, C.; Yang, G.; Li, H.; Du, D.; Lin, Y. *Anal. Chem.* **2015**, *87*, 230–249.
(4) Lim, S. A.; Ahmed, M. U. *RSC Adv.* **2016**, *6*, 24995–25014.
(5) Valera, E.; Hernández-Albors, A.; Marco, M. P. *TrAC - Trends Anal. Chem.* **2016**, *79*, 9–22.
(6) Hernández-Santos, D.; González-García, M. B.; García, A. C. *Electroanalysis* **2002**, *14*, 1225–1235.
(7) Guo, S.; Wang, E. *Nano Today* **2011**, *6*, 240–264.
(8) Omidfar, K.; Khorsand, F.; Azizi, M. D. *Biosens. Bioelectron.* **2013**, *43*, 336–347.
(9) Cao, X.; Ye, Y.; Liu, S. *Anal. Biochem.* **2011**, *417*, 1–16.
(10) Kokkinos, C.; Economou, A. *Anal. Chim. Acta* **2017**, *961*, 12–32.
(11) Ambrosi, A.; Castañeda, M. T.; Killard, A. J.; Smyth, M. R.; Alegret, S.; Merkoçi, A. *Anal. Chem.* **2007**, *79*, 5232–5240.
(12) Leng, C.; Lai, G.; Yan, F.; Ju, H. *Anal. Chim. Acta* **2010**, *666*, 97–101.
(13) Omidfar, K.; Zarei, H.; Gholizadeh, F.; Larijani, B. *Anal. Biochem.* **2012**, *421*, 649–656.
(14) González-García, M. B.; Fernández-Sánchez, C.; Costa-García, A. *Biosens. Bioelectron.* **2000**, *15*, 315–321.
(15) Xu, Q.; Yan, F.; Lei, J.; Leng, C.; Ju, H. *Chem. - A Eur. J.* **2012**, *18*, 4994–4998.
(16) Pinijsuwan, S.; Rijiravanich, P.; Somasundrum, M.; Surareungchai, W. *Adv. Eng. Mater.* **2010**, *12*, 649–653.
(17) Hernández-Santos, D.; González-García, M. B.; Costa.-García. A. *Electrochim. Acta* **2000**, *46*, 607–615.
(18) Authier, L.; Grossiord, C.; Brossier, P.; Limoges, B. *Anal. Chem.* **2001**, *73*, 4450–4456.
(19) Wang, J.; Xu, D.; Kawde, A. N.; Polsky, R. *Anal. Chem.* **2001**, *73*, 5576–5581.
(20) Ozsoz, M.; Erdem, A.; Kerman, K.; Ozkan, D.; Tugrul, B.; Topcuoglu, N.; Ekren, H.; Taylan, M. *Anal. Chem.* **2003**, *75*, 2181–2187.
(21) Ho, J. a; Chang, H. C.; Shih, N. Y.; Wu, L. C.; Chang, Y. F.; Chen, C. C.; Chou, C. *Anal Chem* **2010**, *82*, 5944–5950.
(22) Dequaire, M.; Degrand, C.; Limoges, B. *Anal. Chem.* **2000**, *72*, 5521–5528.
(23) Costa, M. M. Da; La Escosura-Muñiz, A. De; Merkoçi, A. *Electrochem. commun.* **2010**, *12*, 1501–1504.
(24) de la Escosura-Muñiz, A.; Sánchez-Espinel, C.; Díaz-Freitas, B.; González-Fernández, A.; Maltez-da Costa, M.; Merkoçi, A. *Anal. Chem.* **2009**, *81*, 10268–10274.
(25) Espinoza-Castañeda, M.; de la Escosura-Muñiz, A.; González-Ortiz, G.; Martín-Orúe, S. M.; Pérez, J. F.; Merkoçi, A. *Biosens. Bioelectron.* **2013**, *40*, 271–276.
(26) Mayorga-Martinez, C. C.; Chamorro-Garcia, A.; Merkoçi, A. *Biosens. Bioelectron.* **2015**, *67*, 53–58.
(27) González García, M. B.; Costa García, A. *Bioelectrochemistry Bioenerg.* **1995**, *38*, 389–395.
(28) de la Escosura-Muñiz, A.; Parolo, C.; Maran, F.; Mekoçi, A. *Nanoscale* **2011**, *3*, 3350.
(29) *US Environ. Prot. Agency.Technology-Based Effl. Limitations. Chapter 5 NPDES Permit Writ. Manual. Sept. 2010. Downloaded from https//www.epa.gov/sites/production/files/2015-09/documents/pwm_2010.pdf on 02/02.2018.*
(30) Jonsson, A.; Hjalmarsson, C.; Falk, P.; Ivarsson, M.-L. *Br. J. Cancer* **2016**, *115*, 1–4.
(31) Gustavo González, A.; Ángeles Herrador, M. *TrAC - Trends Anal. Chem.* **2007**, *26*, 227–238.
(32) Matlock, M. M.; Howerton, B. S.; Van Aelstyn, M. A.; Nordstrom, F. L.; Atwood, D. A. *Environ. Sci. Technol.* **2002**, *36*, 1636–1639.
(33) Roberto, F. F. *Miner. Eng.* **2017**, *106*, 2–6.
(34) Nunan, T. O.; Viana, I. L.; Peixoto, G. C.; Ernesto, H.; Verster, D. M.; Pereira, J. H.; Bonfatti, J. M.; Cesar Teixeira, L. A. *Miner. Eng.* **2017**, *108*, 67–70.
(35) Xia, X.; Yang, M.; Wang, Y.; Zheng, Y.; Li, Q.; Chen, J.; Xia, Y. *ACS Nano* **2012**, *6*, 512–522.
(36) Ardao, I.; Comenge, J.; Benaiges, M. D.; Álvaro, G.; Puntes, V. F. *Langmuir* **2012**, *28*, 6461–6467.
(37) Zheng, T.; Bott, S.; Huo, Q. *ACS Appl. Mater. Interfaces* **2016**, *8*, 21585–21594.
(38) Marbella, L. E.; Millstone, J. E. *Chem. Mater.* **2015**, *27*, 2721–2739.
(39) Castellanos, M.; Leira, R.; Serena, J.; Pumar, J. M.; Lizasoain, I.; Castillo, J.; Davalos, A. *Stroke* **2003**, *34*, 40–45.
(40) Morancho, A.; Rosell, A.; García-Bonilla, L.; Montaner, J. *Ann. N. Y. Acad. Sci.* **2010**, *1207*, 123–133.

Table of Contents (TOC) – for TOC only